Dalton Transactions

PAPER

Cite this: *Dalton Trans.*, 2019, **48**, 3695

Fabrication of blue organic light-emitting diodes from novel uranium complexes: synthesis, characterization, and electroluminescence studies of uranium anthracene-9-carboxylate complexes†

Khodabakhsh Darzinezhad,[a] Mostafa M. Amini,*[a] Ezeddin Mohajerani,[b] Mahsa Armaghan,[c] Tim Oliver Knedel,[c] Afshin Abareghi[b] and Christoph Janiak*[c]

In this study, three uranium(VI) complexes, $[UO_2(C_{15}H_9O_2)_2(CH_3CH_2OH)_2]\cdot 2CH_3CH_2OH$ (**1**), $[U_2O_4(C_{15}H_9O_2)_2(CH_3O)_2(CH_3OH)_2]\cdot 2CH_3OH$ (**2**), and $[U_2O_4(C_{15}H_9O_2)_4(CH_3OH)_2]\cdot 2H_2O$ (**3**), were prepared by reacting anthracene-9-carboxylic acid with uranyl acetate dihydrate using various ligand to uranyl acetate ratios in different solvents. The infrared and UV-Vis spectra along with elemental and thermal analyses showed the formation of mono- and dinuclear anthracene-9-carboxylate complexes of uranium. A 1 to 3 molar ratio of uranyl acetate to anthracene-9-carboxylic acid in ethanol resulted in the formation of the mononuclear complex **1**, whereas a 1 to 2 and 1 to 3 molar ratio of uranyl acetate to anthracene-9-carboxylic acid in methanol produced the dinuclear complexes **2** and **3**, respectively. Single-crystal structure determinations of **1**, **2** and **3** revealed hexagonal bipyramidal geometries for the mononuclear uranium complex of **1** and a pentagonal geometry for the dinuclear uranium complexes of **2** and **3**. The single-crystal structures of complexes **2** and **3** showed π–π interactions in contrast to complex **1**. The strong π–π interactions in complex **2** and **3** lead to an enhanced photoluminescence intensity in comparison with **1** without π–π interaction. The optical properties of the prepared complexes are associated with the ligand-induced resonant system. The fluorescent uranium complex **1** that showed a blue emission upon excitation at 270 nm was used for the fabrication of a blue organic light-emitting diode (BOLED), an industrially important OLED, using a simple solution-process fabrication method.

Received 18th December 2018,
Accepted 14th February 2019

DOI: 10.1039/c8dt04981e

rsc.li/dalton

Introduction

The light industry is several million dollars in today's market, and organic light-emitting diodes (OLEDs) are rapidly replacing past optical systems. The fundamental phenomenon on which OLEDs operate is electroluminescence. In electroluminescence, electrical energy is converted into photons and light is generated upon applying an electric current. These devices continuously emit their light in all directions.[1]

After the work of C. W. Tang and co-workers in 1987 on OLEDs,[2] there have been numerous studies in industries and research laboratories. The applications of OLEDs cover a full range of utilization from full color flexible, flat-panel, and color large-area flat panel displays, lighting sources in mobile phones, laptops, television sets, and digital cameras to the energy source for solid-state lightings. All these applications are possible due to some of their unique advantages such as being light weight, high contrast, flexibility, secure processing, low cost and easy processability and unlike liquid crystal displays (LCDs) they do not need backlighting, polarizers, and diffusers. These OLEDs can be used in aircraft, automobiles, portable devices, audio components, navigation instruments, locating maps, and for decorative environmental illumination purpose.[3–7]

Structurally, OLEDs are multi-layered, including hole transport layers, electron injection-transport layers, pigments, and hosts. Polymeric, molecular compounds or metal complexes are used in the fabrication of these layers. A typical way to construct standard OLEDs is using the partial energy transfer from a host to emitters. By the recombination of electrons and

[a]*Department of Chemistry, Shahid Behehti University, G.C., Tehran 1983963113, Iran. E-mail: m-pouramini@sbu.ac.ir; Fax: +9-21-22431663; Tel: +98-21-29903109*
[b]*Laser and Plasma Research Institute, Shahid Beheshti University, G.C., 1983963113 Tehran, Iran*
[c]*Institut für Anorganische Chemie und Strukturchemie Heinrich-Heine-Universität, D-40204 Düsseldorf, Germany. E-mail: janiak@uni-duesseldorf.de*

†Electronic supplementary information (ESI) available: Crystal data and structure refinement, selected bond lengths and bond angles, intermolecular ring-interactions in the structures **1–3**, photophysical data, IR spectra, TGA diagrams, fully labelled structure drawings of **1–3**, UV and PL spectra, formulae of BOLED materials. CCDC 1861818 (**1**), 1861820 (**2**) and 1861821 (**3**). For ESI and crystallographic data in CIF or other electronic format see DOI: 10.1039/c8dt04981e

holes, it is possible to obtain electroluminescence in different materials. In this study, uranium complexes were used as pigments in the construction of the OLEDs, which lead to the making of the blue organic light-emitting diodes (BOLEDs). Interestingly, BOLEDs are essential for constructing white organic light-emitting diodes (WOLEDs), which are very popular in the industry. WOLEDs, typically, include either two complementary colors (blue and orange/yellow) or three primary colors (red, blue and green).[8–11]

Uranium complexes have various applications including catalysis,[12] selective dye adsorption,[13] carbon dioxide activation,[14] magnetism,[15] and other applications.[16] Although the optical properties of transition metals and lanthanides have been investigated extensively, there are only limited numbers of, albeit seminal, studies on the photophysical or optical properties of actinides, in particular uranyl complexes,[17–20] despite the fact that they have a quite established chemistry. Considering that actinides exhibit unique chemical behaviour compared to the other groups in the periodic table, exploring their optical character is captivating.[21–23]

Uranyl, UO_2^{2+} complexes show a broad photoluminescent emission between 400 nm and 650 nm.[24,25] This broad emission is caused by the electron transfer from an oxygen orbital to a vacant uranium 5f orbital. If the equatorially coordinated organic ligands have a π-conjugation system, the UV-Vis spectra of these uranyl complexes become complicated, due to charge transfer from the organic ligand. The π-conjugated aromatic organic ligands influence the ligand-centred (LC) emission transitions, facilitate energy transfer, and consequently, influence the fluorescence wavelength by changing its position.[26–29]

The UO_2^{2+} ion has a linear structure with the uranium oxidation state of (VI). The uranyl moiety is the central part in most of the uranium complexes, in which, their oxygen atoms are axially located, and linkers, other organic ligands, and solvents are equatorially coordinated. Uranyl complexes as illustrated in Scheme 1 adopt various coordination geometries, including tetragonal bipyramidal (a), pentagonal bipyramidal (b) and hexagonal bipyramidal (c).[30–32] In addition to a monomeric structure, uranium complexes can adopt dimeric, trimeric and polymeric,[33–36] and metal–organic framework structures (MOFs),[37–42] depending on their equatorially coordinated groups. There are no reports on the formation of complexes between uranium and anthracene-9-carboxylic acid. However, there are some limited reports on the complex of this ligand with lanthanides.[43–47]

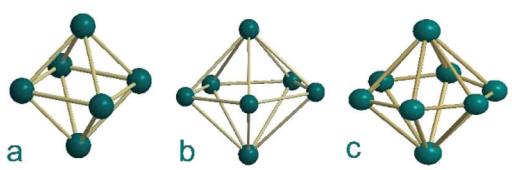

Scheme 1 Three common coordination geometries of uranyl complexes. The two trans-positioned axial atoms correspond to the two O atoms of the UO_2 group.

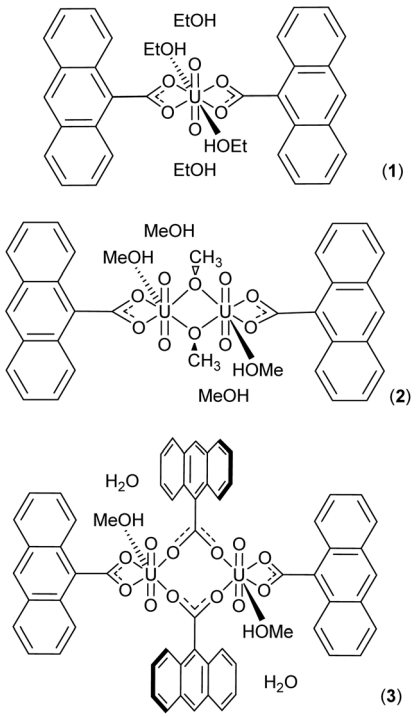

Scheme 2 Structure drawings of complexes **1**, **2** and **3**.

Investigation of the optical properties of the anthracene-9-carboxylate complexes of uranium would be interesting due to the combined presence of an actinide atom and a ligand with a conjugated π-system. In the present study, deprotonated anthracene-9-carboxylic acid is used as a ligand to synthesise three new uranium complexes. All the prepared compounds, $[UO_2(C_{15}H_9O_2)_2(CH_3CH_2OH)_2]\cdot 2CH_3CH_2OH$ (**1**), $[U_2O_4(C_{15}H_9O_2)_2(CH_3O)_2(CH_3OH)_2]\cdot 2CH_3OH$ (**2**), and $[U_2O_4(C_{15}H_9O_2)_4(CH_3OH)_2]\cdot 2H_2O$ (**3**) (Scheme 2), were characterized by single-crystal X-ray diffraction. Complex **1** was used as a pigment to fabricate a blue organic light emitting diode, employing solution-process methods.

Results and discussion

Synthesis and characterization

The reaction of anthracene-9-carboxylic acid with uranium acetate dihydrate in a 3 : 1 ratio in ethanol in a solvothermal chamber resulted in the formation of mononuclear $[UO_2(C_{15}H_9O_2)_2(CH_3CH_2OH)_2]\cdot 2CH_3CH_2OH$ (**1**), whereas the 2 : 1 stoichiometric ratio in methanol yielded the dinuclear complex $[U_2O_4(C_{15}H_9O_2)_2(CH_3O)_2]\cdot 2CH_3OH$ (**2**) with bridging methanolato and terminal anthracene-9-carboxylate ligands. Interestingly, when the stoichiometric ratio 3 : 1 and the reaction was carried out in methanol under the same reaction conditions, also a dinuclear complex of formula $[U_2O_4(C_{15}H_9O_2)_4(CH_3OH)_2]\cdot 2H_2O$ (**3**) formed, but with two bridging and two terminal anthracene-9-carboxylate ligands (Scheme 2). According to the single-crystal X-ray structure ana-

lyses (see below) in all the prepared complexes the anthracene-9-carboxylate moieties act as bidentate chelating or bridging ligands regardless of the metal-to-ligand ratio. The dinuclear complex **3** with bridged anthracene-9-carboxylate ligands was only formed when a 3 : 1 ligand-to-metal ratio was used. Attempts for the preparation of a complex with a 2 : 1 ligand-to-metal ratio in ethanol did not result in the formation of a crystal. It seems that the acidity/basicity of the solvent has led to the changes in the structures of the synthesized complexes. Ethanol in comparison with anthracene-9-carboxylic acid and methanol is more basic; therefore, its deprotonation for coordination as the ethanolate, akin to methanolate in **2**, is unfavourable. Uranium tends to exhibit a high coordination number in all of these compounds by utilizing coordinating solvents, and interestingly, the reaction in non-coordinating solvents did not lead to successful results. All the prepared complexes were characterized by FTIR, TGA, elemental analysis and single-crystal X-ray diffraction.

FT-IR spectra of the complexes are shown in Fig. S1, ESI.† As can be seen, the stretching vibration bands of U–O for compounds **1**, **2** and **3** appeared at 874, 953; 779, 908; and 875, 952 cm^{-1}, respectively. The bands at about 1300 and 1400 cm^{-1} in the spectra of the complexes are associated with the stretching vibrations of the C=C bond of the anthracene-9-carboxylate component in the complexes.[48–50] The bands in the range of 1626–1526 cm^{-1} are assigned to the asymmetric and symmetric stretching vibrations of C=O of the anthracene-9-carboxylate ligand. These bands are significantly shifted to lower energy in comparison with those of free anthracene-9-carboxylic acid, which shows its coordination as a carboxylate ligand to uranium. These characteristic IR bands, ν_{as} and ν_{s}, of complexes **1**, **2** and **3** appeared at 1626, 1530; 1623, 1526; and 1626, 1529 cm^{-1}, respectively. The anthracene-9-carboxylic acid stretching vibration band of the carboxylic OH at 3033 cm^{-1} disappeared upon complex formation and also confirmed carboxylate formation with coordination to uranium.[51,52]

The thermal stability of complexes was investigated by TGA and the thermograms are illustrated in Fig. S2 (ESI†). The distinct mass loss of about 40% at 430 °C is attributed to the simultaneous decomposition and combustion of the organic groups of the complexes. Such a high thermal stability is an advantage in the fabrication of the optical device which requires a high processing temperature.

Crystal structure of $[UO_2(C_{15}H_9O_2)_2(CH_3CH_2OH)_2]\cdot 2CH_3CH_2OH$ (1). Complex **1** crystallizes in the monoclinic space group $P2_1/c$. The asymmetric unit consists of two ethanol crystal solvent molecules and a complete mononuclear complex molecule, which includes one uranium atom, two oxido ligands, two coordinated ethanol and two terminal anthracene-9-carboxylate acid ligands. The latter are coordinated to uranium as bidentate chelating ligands. Two equatorially coordinated ethanol molecules assist the formation of a hexagonal bipyramidal structure in which the oxido ligands are *trans* positioned with respect to each other (Fig. 1). The two oxido ligands have an approximately linear orientation with an angle of 179.51(11)° and the bond lengths of U–O1 and U–O2 were 1.747(2) and 1.750(2) Å, respectively. The crystallographic data and selected bond lengths and bond angles are listed in Tables S1 and S2 (ESI†), respectively.

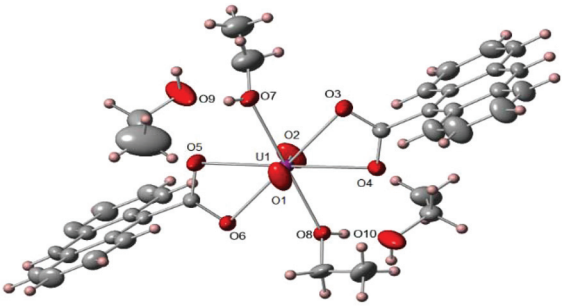

Fig. 1 X-ray molecular structure of $[UO_2(C_{15}H_9O_2)_2(CH_3CH_2OH)_2]$ 2 (CH_3CH_2OH) (**1**) with partial atom labeling showing coordination around uranium atoms. The thermal displacement ellipsoids are drawn at the 50% probability level.

Crystal structure of $[U_2O_4(C_{15}H_9O_2)_2(CH_3O)_2(CH_3OH)_2]\cdot 2CH_3OH$ (2). Complex **2** crystallizes in the triclinic space group $P\bar{1}$. The asymmetric unit consists of half of the dinuclear complex molecule and includes one uranium atom, two oxido ligands, a coordinated methanol and methoxy group and one terminal anthracene-9-carboxylate ligand. In addition, there is one methanol crystal solvent molecule in the asymmetric unit. As shown in Fig. 2, the geometry around uranium atoms is pentagonal bipyramidal. The anthracene-9-carboxylate ligand is coordinated to uranium as a bidentate chelate ligand. In the inversion-symmetric dinuclear complex, two methoxy groups act as bridging ligands between the two uranium atoms. As expected, the two oxido ligands on each uranium atom are *trans* positioned to each other in an approximately linear orientation with an angle of 176.8(6)° similar to that of compound **1**. The U–O3 and U–O4 bond lengths are 1.739(13) and 1.758(13) Å, respectively, and are almost identical to those of compound **1**. The distance between two uranium atoms is 3.81 Å. The crystallographic data and selected bond lengths and angles are listed in Tables S1 and S3 (ESI†), respectively.

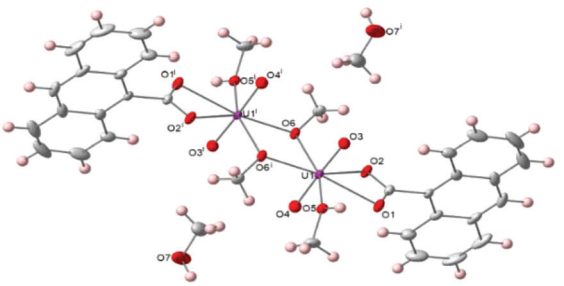

Fig. 2 X-ray molecular structure of $[U_2O_4(C_{15}H_9O_2)_2(CH_3O)_2(CH_3OH)_2]\cdot 2CH_3OH$ (**2**) with a partial atom-labeling scheme. The thermal displacement ellipsoids are drawn at the 50% probability level. Symmetry transformation $i = 1 - x, 1 - y, 1 - z$.

Crystal structure of $[U_2O_4(C_{15}H_9O_2)_4(CH_3OH)_2]\cdot 2H_2O$ (3). Single-crystal structure determination shows that the dinuclear complex **3** crystallizes in the triclinic space group $P\bar{1}$. The asymmetric unit comprises half of the dinuclear complex of **3** and consists of one uranium atom, two oxido ligands, one cooordinated methanol, and two anthracene-9-carboxylate ligands. There is one crystal water molecule in the asymmetric unit. The coordination geometry around uranium atoms, similar to complex **2**, can best be described as pentagonal bipyramidal (Fig. 3). In the complete dinuclear complex, four anthracene-9-carboxylate ligands are coordinated to the two uranium atoms, two in the form of bidentate chelating ligands in the equatorial position and two in the form of bidentate bridging ligands between the uranium atoms. Similar to the molecular structures of **1** and **2**, a methanol solvent molecule is coordinated to uranium and assists in the formation of a high coordination number. The oxido ligands are *trans* to each other, and the O3–U–O4 angle with a value of 175.8(9)° almost is linear. The U–O3 and U–O4 bond lengths are 1.71(2) and 1.61(2) Å, respectively. Notably, the distance between the two uranium atoms in **3** is 5.45 Å, which is significantly larger than that in compound **2** and can be attributed to the bridging anthracene-9-carboxylate ligand in **3** in comparison with the methoxy ligand in **2**. The crystallographic data and selected bond lengths and bond angles are listed in Tables S1 and S4 (ESI†), respectively.

Complexes **2** and **3** are analogues in terms of the ligand arrangement around the metal atoms and the space group, but compound **1** is different concerning the crystal system and space group.

Supramolecular interactions are observed between the complexes (and crystal solvent molecules) in the crystals of **1**, **2** and **3**. Such supramolecular interactions are effective in forming the final structure and contribute to the stability of the structure, with the crystal solvent molecules filling empty spaces between the main metal–ligand complex units. In the crystals of **2** and **3**, offset π–π stacking interactions were observed (details in Table S5, ESI†). Notably π-π interactions were not found in the crystal packing of **1**. In addition to π–π interactions, C–H–π interactions were detected in all three crystals (details in Table S6, ESI†). The molecular structures of the complexes with the complete atom labelling are illustrated in Fig. S3–S5 (ESI†).[53]

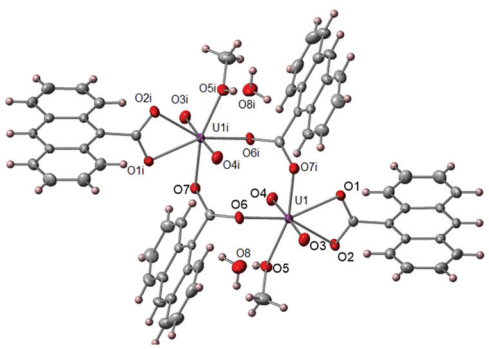

Fig. 3 X-ray molecular structure of $[U_2O_4(C_{15}H_9O_2)_4(CH_3OH)_2]\cdot 2H_2O$ (**3**) with partial atom labeling. Displacement ellipsoids are drawn at the 50% probability level. Symmetry transformation $i = 1 - x, 1 - y, -z$.

UV-Vis absorption spectra

The absorption spectrum of the anthracene-9-carboxylic acid ligand at ambient temperature features two broad bands at 252 and 364 nm, which correspond to the K-band and B-band, respectively (Fig. S6, ESI†). The K-band at the lower wavelength and with the higher molar absorption coefficient and the B-band at the higher wavelength and with the lower molar absorption coefficient are associated with the π → π* transitions.[54,55] In complexes **1** and **2**, two anthracene-9-carboxylate ligands are present in contrast to four anthracene-9-carboxylates in complex **3**. In complex **1**, each uranium atom is coordinated to two anthracene-9-carboxylate ligands, and in complex **2**, each uranium atom is coordinated to only one anthracene-9-carboxylate ligand. Absorption and photoluminescence spectra of **1–3** were recorded in THF under the same conditions to investigate the effect of the number of the anthracene-9-carboxylate ligands on the photoluminescence spectra of the complexes. Fig. 4 shows the UV-Vis absorption spectra of all complexes, recorded in 0.001 mM concentration. As manifested, K-bands and B-bands of all complexes, which are also associated with the π → π* transitions, and well defined in shape, appear at 250, 368; 256, 368 and 255, 367 nm for **1**, **2** and **3**, respectively. These bands are slightly shifted to longer wavelengths compared to the free ligands. Although both K- and B-bands of all complexes appear in the same regions, their molar absorption coefficients are different, and are in order of **1** > **3** > **2**, and of **3** > **1** > **2** for K- and B-bands, respectively. The order of intensities can be attributed to the number of anthracene ligands in the complexes. According to the crystal structures, the uranium atom in **1** and **3** is bound to two anthracene ligands, while the uranium atom in **2** has only one anthracene ligand. Therefore, it can be concluded that an increased number of coordinated resonance systems will lead to higher absorption intensity. The presence of these absorption bands in the spectrum of the complexes indicates the vital role of the anthracene-9-carboxylate ligand-induced resonance system in the optical properties of the prepared complexes.

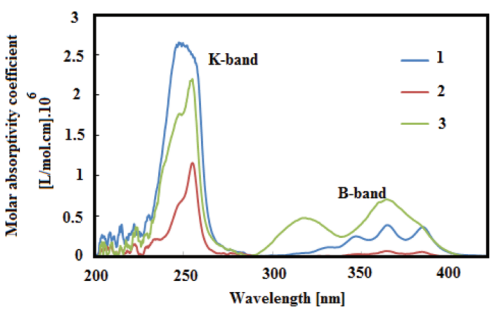

Fig. 4 UV-Vis spectra of complexes **1**, **2** and **3** in THF.

Photoluminescence studies

The photoluminescence spectra of the complexes **1**, **2** and **3** were recorded at 273 K in THF using an excitation wavelength of 270 nm with the same intensity of the radiation source for all three complexes (Fig. 5). The observed emission spectra are in the expected ranges. All compounds showed a similar photoluminescence spectral pattern in the range of 350–550 nm,[56] and the intensities in the PL spectra are in the order of **3** > **1** > **2**. It should be noticed that the PL intensities are corrected according to the molar absorptivity coefficients. The order of the PL intensities, similar to the absorption spectra, can be attributed to the number of anthracene ligands, which are bound to the uranium atom in the complexes. Notably, it is expected to observe the metal-centred emission bands in the PL and EL spectra of the complexes, but since the PL and EL emission bands of the anthracene-9-carboxylate ligand are dominating, they obscure the PL and EL metal-centred emission. For verification, the PL spectra of anthracene-9-carboxylic acid (Fig. S7, ESI†), uranyl acetate dihydrate (Fig. S8, ESI†), and the final complexes were recorded (Fig. 5). The PL spectra of the non-deprotonated ligand, uranyl acetate, and the complexes show bands in the 400–550, 550–700 and 400–550 nm regions, respectively. It is evident that the PL spectra of the complexes are in the same region as anthracene-9-carboxylic acid and not in the region of uranyl acetate, albeit with much higher intensity for the acid ligand emission band. This confirms that the metal-centred emission band is obscured by the emission of the complex. Apparently, ligand-centred (LC) transitions in the conjugated system facilitate the emission. The photophysical properties of the complexes along with the photophysical properties of anthracene-9-carboxylic acid and uranyl acetate are listed in Table S7 (ESI†).

Since the supramolecular π–π and C–H–π interactions, involving the anthracene moiety, play an important role in the solid state,[57–61] an attempt has been made to record solid-state PL spectra of the complexes to possibly ascertain the influence of the solid *versus* solution environment. As shown in Fig. 6, the order of PL intensity in the solid-state changed to **2** > **3** > **1**. This difference in the order of the PL spectral intensity can be attributed to the supramolecular interactions in complexes. The single-crystal structure of complexes shows π–π stacking interactions only for complex **2** and **3**. Furthermore, centroid–centroid π–π ring-interactions in complex **2** (Table S5†) are shorter than in complex **3**. Evidently, π–π stacking interactions in the solid state in complex **2** enhance the PL spectral intensity in contrast to the PL spectrum in solution where such supramolecular π–π stacking between adjacent complexes does not exist. In other words, the PL intensity in solution, which is governed by the number of anthracene rings to uranium atoms of complexes, changed in the solid-state and secondary interactions became dominant. Notably, the complex **1**, second in order of intensity in solution, became third in the solid state, which has no π–π stacking interaction.

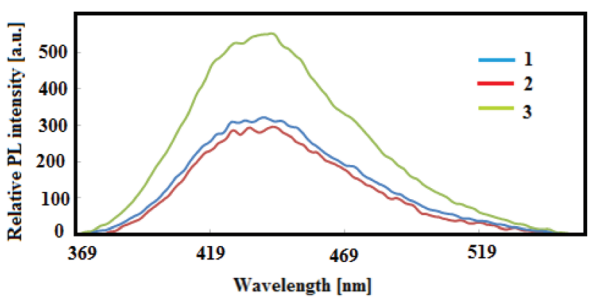

Fig. 5 Photoluminescence spectra of complexes **1**, **2** and **3** in THF at an excitation wavelength of 270 nm at 273 K.

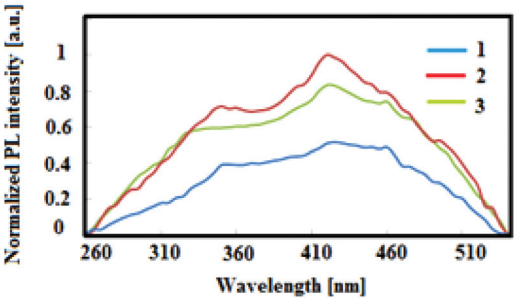

Fig. 6 Normalized solid-state photoluminescence spectra of complexes **1**, **2** and **3** at an excitation wavelength of 270 nm at 273 K.

Blue organic light-emitting devices

To investigate the effectiveness of the synthesized complexes to function as a blue fluorescent material, complex **1** was used as a pigment to fabricate a blue OLED. The chemical structures of the compounds that were used to fabricate the BOLED are shown in Scheme S1 (ESI†), and the structure of the BOLED is illustrated in Fig. 7. BCP was used as a hole blocker and was coated on PVK : TPD : PBD : complex **1** through the vapor deposition method at 1 Å s^{-1} at a thickness of 8 nm. Silver metal then was coated on BCP through vapor deposition at a thickness of 120 nm. The active area of the

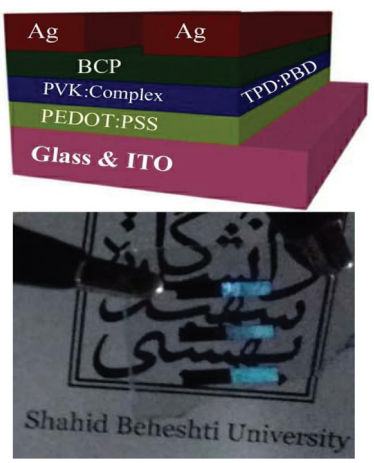

Fig. 7 The device structure of the BOLED.

prepared device was 3 × 1.5 mm^2. The fundamental structure of the BOLED was glass/ITO/PEDOT : PSS (60 nm)/PVK : TPD : PBD : complex **1** (65 nm)/BCP (8 nm)/Ag (120 nm). It should be mentioned that five attempts for using the best performing complex **3** in a device were not successful. Notably, the fabricated device emitted powerful light but after couple minutes burned out. The instability of the device with complex **3** was attributed to the presence of water in the complex. The effect of water trapped in the complex in the quenching of photoluminescence has been noticed before.[62,63]

Electroluminescence studies

The electroluminescence (EL) spectrum of the fabricated device at 25 V is illustrated in Fig. 8. Results show a good fit with the photoluminescence (PL) spectrum and the maximum observed absorption wavelength in the spectrum is 500 nm. The current–voltage (*JV*) and luminance–voltage (*LV*) curves of the prepared BOLED show that the highest current occurs at a voltage of 22 V with the maximum amount of luminance at this voltage (Fig. 9).

The chromaticity diagram of the fabricated devices is illustrated in Fig. 10. As can be seen, the CIE coordinates for the devices that contain complex **1** are rather far from c_x = 0.23 and c_y = 0.37, the ideal blue point coordinates. As shown in Fig. 10, the emission color of the complex is dominated by the ligand; therefore, the emission color can be adjusted by careful design and engineering of the structure of the ligand. Finally, since the electroluminescence spectrum of complex **1** is confirmed by the CIE chromaticity diagram, one can conclude that the synthesized uranium complex **1** with its broad emission spectrum is a suitable material for the fabrication of high-quality blue light sources. Table 1 summarizes the characterization of the prepared BOLED device. Turn-on voltage and current efficiency for the BOLED based on complex **1** were calculated as 7 V and 2.2 cd $Å^{-1}$, respectively.[64,65]

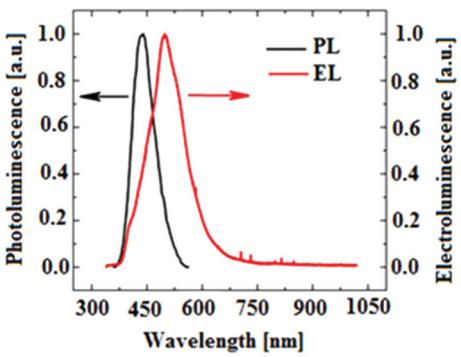

Fig. 8 Electroluminescence and photoluminescence spectra of complex **1** at 25 eV.

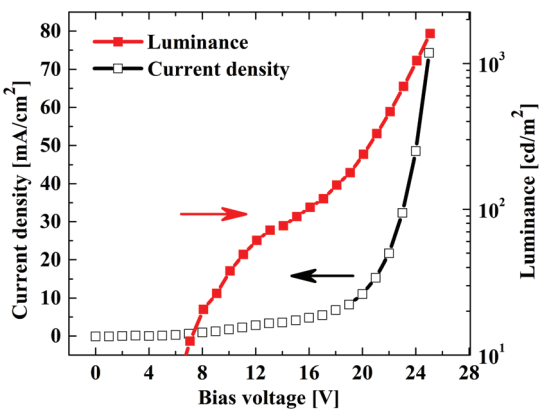

Fig. 9 Current–voltage (*JV*) and luminance–voltage (*LV*) curves of the fabricated BOLED.

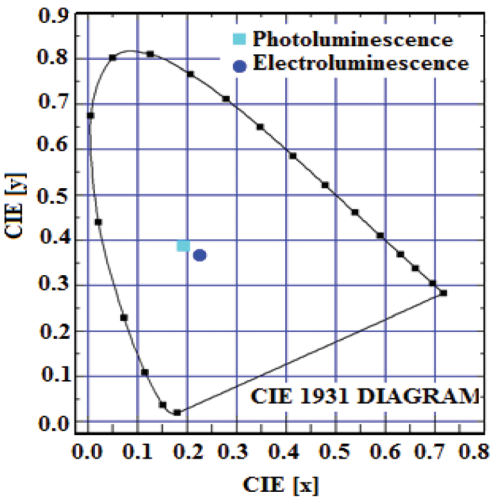

Fig. 10 Variation in the CIE 1931 chromaticity coordinates for the BOLED.

Experimental section

Materials and measurements

Caution! $^{238}UO_2(acetate)_2{\cdot}2H_2O$ is toxic and somewhat radioactive.

We used depleted uranium in our work (^{238}U). Uranyl acetate dihydrate and anthracene-9-carboxylic acid were purchased from Merck and Aldrich and used without further purification. *N*,*N*′-Bis(3-methylphenyl)-*N*,*N*′-diphenylbenzidine (TPD), 2,9-dimethyl-4,7-diphenyl-1,10-phenanthroline (BCP), 2-phenyl-5-(4-biphenylyl)-1,3,4-oxadiazole (PBD), poly(vinylcarbazole) (PVK), 4-(dicyanomethylene)-2-methyl-6-(4-dimethylaminostyryl)-4*H*-pyran (DCM), poly(3,4-ethylenedi-oxythiophene) poly(styrene sulfonate) (PEDOT : PSS), and indium tin oxide (ITO) which are used for the fabrication of the OLEDs were acquired from Aldrich. Methanol and ethanol were dried and distilled under dried nitrogen using standard procedures.[66] Melting points were recorded with an Electrothermal 9200 melting point apparatus. Microanalyses, CHN, were conducted with a Thermo Finnigan Flash-1112EA CHNS elemental analyzer. FTIR spectra in the range of 4000 to

Table 1 Device characteristics of the BOLED based on complex **1** at 25 V

Peak emiss.	CIE[a] [x, y]	FWHM[b]	Turn-on voltage	Current density	Lumin.	Current effic.
514.3 nm	(0.226, 0.367)	113.1 nm	7 V	74.3 mA cm^{-1}	1601 cd m^{-2}	2.2 cd $Å^{-1}$

[a] Commission International del'Eclairage. [b] Full width at half maximum.

250 cm^{-1} were recorded on a Bomem MB-series FTIR spectrophotometer with a spectral resolution of 4 cm^{-1} using KBr pellets of complexes. Thermal analysis (TGA) of complexes was performed using a Bahr STA-504 instrument at a heating rate of 10 °C min^{-1} under air. The photoluminescence spectra in solution were recorded in THF at 273 K with a concentration of 1.0×10^{-6} mol L^{-1} and an excitation wavelength of 270 nm utilizing a quartz cell on a USB2000 spectrophotometer and in solid-state at room temperature by the same excitation wavelength using a JASCO FP-6500 spectrofluorometer. A Shimadzu 2100 spectrophotometer was used to obtain UV-Vis spectra. The thickness of the samples was measured by using a Dektak 8000 profilometer. USB2000 and a HR4000 Ocean Optics spectrometer were used to measure the electroluminescence of the fabricated OLEDs. A Keithley source-measure unit model 2400 was used to check the current–voltage–luminance characteristics.

X-ray crystallography

The X-ray data sets were obtained on a Bruker Kappa APEX2 CCD diffractometer with a microfocus tube, Mo-Kα radiation (λ = 0.71073 Å), ω- and φ-scan. Data collection was carried out with APEX2 software, cell refinement and data reduction with SAINT,[67] and experimental absorption correction with SADABS.[68] Structures were solved by direct methods using SHELXT2014/7 and refined by full-matrix least squares of F^2 with SHELXL2014/7.[69] All non-hydrogen atom positions were refined with anisotropic displacement parameters. All hydrogen atoms were positioned geometrically (with C–H = 0.95 Å for aromatic and aliphatic CH, 0.99 Å for CH_2, and 0.98 Å for CH_3 and riding models (AFIX 43, 23 and 137, respectively), with $U_{iso}(H) = 1.2U_{eq}$ (CH, CH_2) and $1.5U_{eq}$ (CH_3). The hydrogen atoms for the water molecule in structure **3** were found from the electron density map. Graphics were drawn with DIAMOND.[70] Crystallographic data and refinement parameters for $[UO_2(C_{15}H_9O_2)_2(CH_3CH_2OH)_2]\cdot 2CH_3CH_2OH$ (**1**), $[U_2O_4(C_{15}H_9O_2)_2(CH_3O)_2(CH_3OH)_2]\cdot 2CH_3OH$ (**2**), and $[U_2O_4(C_{15}H_9O_2)_4(CH_3OH)_2]\cdot 2H_2O$ (**3**) are listed in Table S1 (ESI†).

Syntheses of complexes

Synthesis of $[UO_2(C_{15}H_9O_2)_2(CH_3CH_2OH)_2]\cdot 2CH_3CH_2OH$ (1). Uranyl acetate dihydrate (0.05 mmol, 0.021 g) [**Caution!** $^{238}UO_2(acetate)_2\cdot 2H_2O$ is toxic and somewhat radioactive] and anthracene-9-carboxylic acid (0.15 mmol, 0.0333 g) were mixed and sonicated in ethanol for 10 min. Then the mixture was sealed into a 25 mL glass tube and heated at 80 °C. After 9 days, the tube was cooled to room temperature in ambient air, and the brown crystals were collected, washed with deionized water, dried at room temperature and used for characterization (yield 67.6%, m.p. >250 °C). Anal. calc. for $C_{34}H_{30}O_8U$: C, 50.75; H, 3.76. Found: C, 50.95; H, 3.42. IR (KBr pellet, cm^{-1}): 3434, 1626, 1530, 1381, 1039, 953, 874, 785, 643, 601, 562, 521.

Synthesis of $[U_2O_4(C_{15}H_9O_2)_2(CH_3O)_2(CH_3OH)_2]\cdot 2CH_3OH$ (2). Uranyl acetate dihydrate (0.10 mmol, 0.042 g) and anthracene-9-carboxylic acid (0.20 mmol, 0.044 g) were mixed and sonicated in methanol. After being mixed for 10 min, the mixture was sealed into a 25 mL glass tube and heated at 80 °C. After 9 days, the tube was cooled down to room temperature naturally, and the brown crystals were collected, washed with ultrapure water, dried at room temperature and then used for characterization (yield 39.6%, m.p. >250 °C). Anal. calc. for $C_{34}H_{32}O_{12}U_2$: C, 36.83; H, 2.91. Found: C, 36.18; H, 3.28. IR (KBr pellet, cm^{-1}): 3509, 1623, 1526, 1488, 1445, 1393, 1320, 1275, 1145, 994, 908, 779, 733, 643, 558, 507.

Synthesis of $[U_2O_4(C_{15}H_9O_2)_4(CH_3OH)_2]\cdot 2H_2O$ (3). Uranyl acetate dihydrate (0.50 mmol, 0.21 g) and anthracene-9-carboxylic acid (1.50 mmol, 0.333 g) were mixed and sonicated in methanol. After being mixed for 10 min, the mixture was sealed into a 25 mL glass tube and heated at 80 °C. After 9 days, the tube was cooled down to room temperature naturally, and the brown crystals were collected, washed with ultrapure water, dried at room temperature and then used for characterization (yield 43.5%, m.p. >250 °C). Anal. calc. for $C_{62}H_{48}O_{16}U_2$: C, 48.83; H, 3.17. Found: 48.51; 3.08. IR (KBr pellet, cm^{-1}): 3409, 3052, 1626, 1529, 1380, 1228, 1012, 952, 875, 785, 643, 597, 557, 518.

Fabrication of the BOLED

First, the ITO substrate was cleaned with ethanol, acetone, isopropanol, detergent, and deionized water for 14 min in an ultrasonic bath. Then the hole injection layer, PEDOT : PSS, was spin-coated on the ITO substrate at a thickness of 60 nm and was heated in an oven for 30 min at 120 °C. Following this step, PVK : TPD : PBD : complex **1** with a ratio of 100 : 10 : 40 : 5 (3.22 mg: 0.32 mg: 1.29 mg: 0.16 mg) as the light emitting layer was spin-coated on PEDOT : PSS at a thickness of 65 nm and heated in an oven for 30 min at 110 °C. BCP was used as a hole blocker and was coated on PVK : TPD : PBD : complex **1** by the vapor deposition method at 1 Å s^{-1} at a thickness of 8 nm. Finally, silver was coated on BCP through vapor deposition at a thickness of 120 nm. The functional area of the fabricated samples was 3 × 1.5 mm^2. The structure of the OLED was ITO/PEDOT : PSS (60 nm)/PVK : TPD : PBD : complex **1** (65 nm)/BCP (8 nm)/Ag (120 nm).[71–74]

Conclusions

In this study, solvothermal and ultrasonic methods were applied to prepare three new uranium complexes from anthracene-9-carboxylic acid. All the prepared complexes were characterized by various techniques. The representative complex (**1**) was utilized as a fluorescent pigment to fabricate the BOLED. The importance of the utilized ligand was supported through photophysical investigation of the prepared complex and the fabricated OLED. Therefore, it is possible, by using an appropriate ligand with actinide series elements, to synthesize complexes and tune their optical properties for the fabrication of highly efficient light sources.

Conflicts of interest

There are no conflicts of interest to declare.

Acknowledgements

We gratefully acknowledge the financial support (grant number S600/43) from the Research Council of Shahid Beheshti University.

Notes and references

1 H. Klauk, *Organic electronics: materials, manufacturing, and applications*, John Wiley & Sons, 2006.
2 C. W. Tang and S. A. VanSlyke, *Appl. Phys. Lett.*, 1987, **51**, 913–915.
3 D. Luo, Y. Yang, L. Huang, B. Liu and Y. Zhao, *Dyes Pigm.*, 2017, **147**, 83–89.
4 Y. Miao, K. Wang, B. Zhao, L. Gao, P. Tao, X. Liu, Y. Hao, H. Wang, B. Xu and F. Zhu, *Nanophotonics*, 2018, **7**, 295–304.
5 Y. Wang, Y. Zhu, G. Xie, H. Zhan, C. Yang and Y. Cheng, *J. Mater. Chem. C*, 2017, **5**, 10715–10720.
6 Z. Wu, J. Luo, N. Sun, L. Zhu, H. Sun, L. Yu, D. Yang, X. Qiao, J. Chen and C. Yang, *Adv. Funct. Mater.*, 2016, **26**, 3306–3313.
7 Z. Yang, Z. Mao, Z. Xie, Y. Zhang, S. Liu, J. Zhao, J. Xu, Z. Chi and M. P. Aldred, *Chem. Soc. Rev.*, 2017, **46**, 915–1016.
8 C. Fan and C. Yang, *Chem. Soc. Rev.*, 2014, **43**, 6439–6469.
9 M. J. Jurow, C. Mayr, T. D. Schmidt, T. Lampe, P. I. Djurovich, W. Brütting and M. E. Thompson, *Nat. Mater.*, 2016, **15**, 85–91.
10 Y. Liu, X. Chen, Y. Lv, S. Chen, J. W. Y. Lam, F. Mahtab, H. S. Kwok, X. Tao and B. Z. Tang, *Chem. – Eur. J.*, 2012, **18**, 9929–9938.
11 J. Yang, J. Huang, Q. Li and Z. Li, *J. Mater. Chem. C*, 2016, **4**, 2663–2684.
12 D. P. Halter, F. W. Heinemann, L. Maron and K. Meyer, *Nat. Chem.*, 2018, **10**, 259.
13 K. Q. Hu, X. Jiang, C. Z. Wang, L. Mei, Z. N. Xie, W. Q. Tao, X. L. Zhang, Z. F. Chai and W. Q. Shi, *Chem. – Eur. J.*, 2017, **23**, 529–532.
14 S. C. Bart, C. Anthon, F. W. Heinemann, E. Bill, N. M. Edelstein and K. Meyer, *J. Am. Chem. Soc.*, 2008, **130**, 12536–12546.
15 P. M. Almond, L. Deakin, A. Mar and T. E. Albrecht-Schmitt, *Inorg. Chem.*, 2001, **40**, 886–890.
16 D. Sun, N. Zhang, Q.-J. Xu, R.-B. Huang and L.-S. Zheng, *Inorg. Chem. Commun.*, 2010, **13**, 859–862.
17 R. L. Belford and E. Rabinowitch, *Spectroscopy and Photochemistry of Uranyl Compounds*, Pergamon Press, Oxford, 1964.
18 R. G. Denning, *J. Phys. Chem. A*, 2007, **111**, 4125–4143.
19 R. Günther and J. Manley, *Archaeologia*, 1912, **63**, 99–108.
20 L. S. Natrajan, *Coord. Chem. Rev.*, 2012, **256**, 1583–1603.
21 F. Baur and T. Jüstel, *J. Lumin.*, 2018, **196**, 431–436.
22 G. R. Dieckmann, A. B. Ellis and E. E. Hellstrom, *J. Electrochem. Soc.*, 1990, **137**, 2331–2335.
23 P. Harvey, A. Nonat, C. Platas Iglesias, L. Natrajan and L. Charbonniere, *Angew. Chem., Int. Ed.*, 2018, **130**, 10069–10072.
24 L. Liang, R. Zhang, N. S. Weng, J. Zhao and C. Liu, *Inorg. Chem. Commun.*, 2016, **64**, 56–58.
25 S. G. Thangavelu, R. J. Butcher and C. L. Cahill, *Cryst. Growth Des.*, 2015, **15**, 3481–3492.
26 L. A. Borkowski and C. L. Cahill, *Cryst. Growth Des.*, 2006, **6**, 2248–2259.
27 M. Frisch and C. L. Cahill, *Dalton Trans.*, 2006, 4679–4690.
28 S. Tsushima, C. Götz and K. Fahmy, *Chem. – Eur. J.*, 2010, **16**, 8029–8033.
29 Y. Z. Zheng, M. L. Tong and X. M. Chen, *Eur. J. Inorg. Chem.*, 2005, 4109–4117.
30 M. B. Andrews and C. L. Cahill, *Chem. Rev.*, 2013, **113**, 1121–1136.
31 Q. J. Pan, G. A. Shamov and G. Schreckenbach, *Chem. – Eur. J.*, 2010, **16**, 2282–2290.
32 S. G. Thangavelu and C. L. Cahill, *Cryst. Growth Des.*, 2015, **16**, 42–50.
33 W. Liu, X. Dai, J. Xie, M. Silver, D. Zhang, Y. Wang, Y. Cai, J. Diwu, J. Wang and R. Zhou, *ACS Appl. Mater. Interfaces*, 2018, **10**, 4844–4850.
34 L. Mei, C.-Z. Wang, L.-Z. Zhu, Z.-Q. Gao, Z.-F. Chai, J. K. Gibson and W.-Q. Shi, *Inorg. Chem.*, 2017, **56**, 7694–7706.
35 L. Mei, Q.-Y. Wu, C.-M. Liu, Y.-L. Zhao, Z.-F. Chai and W.-Q. Shi, *Chem. Commun.*, 2014, **50**, 3612–3615.
36 J. Xie, Y. Wang, M. A. Silver, W. Liu, T. Duan, X. Yin, L. Chen, J. Diwu, Z. Chai and S. Wang, *Inorg. Chem.*, 2018, **57**, 575–582.
37 P. Li, N. A. Vermeulen, X. Gong, C. D. Malliakas, J. F. Stoddart, J. T. Hupp and O. K. Farha, *Angew. Chem., Int. Ed.*, 2016, **55**, 10358–10362.
38 P. Li, N. A. Vermeulen, C. D. Malliakas, D. A. Gómez-Gualdrón, A. J. Howarth, B. L. Mehdi, A. Dohnalkova,

N. D. Browning, M. O'keeffe and O. K. Farha, *Science*, 2017, **356**, 624–627.
39 W. Liu, J. Xie, L. Zhang, M. A. Silver and S. Wang, *Dalton Trans.*, 2018, **47**, 649–653.
40 X. Wang, Y. Wang, X. Dai, M. A. Silver, W. Liu, Y. Li, Z. Bai, D. Gui, L. Chen and J. Diwu, *Chem. Commun.*, 2018, **54**, 627–630.
41 Y. Wang, Z. Liu, Y. Li, Z. Bai, W. Liu, Y. Wang, X. Xu, C. Xiao, D. Sheng and J. Diwu, *J. Am. Chem. Soc.*, 2015, **137**, 6144–6147.
42 Y. Wang, X. Yin, W. Liu, J. Xie, J. Chen, M. A. Silver, D. Sheng, L. Chen, J. Diwu and N. Liu, *Angew. Chem., Int. Ed.*, 2018, **57**, 7883–7887.
43 E. Colacio, J. Ruiz, A. J. Mota, M. A. Palacios, E. Cremades, E. Ruiz, F. J. White and E. K. Brechin, *Inorg. Chem.*, 2012, **51**, 5857–5868.
44 E. Kusrini, R. Adnan, M. I. Saleh, L.-K. Yan and H.-K. Fun, *Spectrochim. Acta, Part A*, 2009, **72**, 884–889.
45 C.-S. Liu, L.-Q. Guo, L.-F. Yan and J.-J. Wang, *Acta Crystallogr., Sect. C: Struct. Chem.*, 2008, **C64**, m292–m295.
46 C.-S. Liu, M. Hu and Q. Zhang, *J. Chem. Crystallogr.*, 2010, **40**, 1002–1005.
47 M. A. Palacios, S. Titos-Padilla, J. Ruiz, J. M. Herrera, S. J. Pope, E. K. Brechin and E. Colacio, *Inorg. Chem.*, 2013, **53**, 1465–1474.
48 C. Engelter, C. L. Knight and D. A. Thornton, *Spectrosc. Lett.*, 1989, **22**, 1161–1172.
49 Q.-J. Pan, Y.-M. Wang, R.-X. Wang, H.-Y. Wu, W. Yang, Z.-M. Sun and H.-X. Zhang, *RSC Adv.*, 2013, **3**, 1572–1582.
50 D. M. Poojary, A. Cabeza, M. A. Aranda, S. Bruque and A. Clearfield, *Inorg. Chem.*, 1996, **35**, 1468–1473.
51 H. A. Azab, S. El-Korashy, Z. Anwar, B. Hussein and G. Khairy, *Spectrochim. Acta, Part A*, 2010, **75**, 21–27.
52 R. M. Silverstein, F. X. Webster, D. J. Kiemle and D. L. Bryce, *Spectrometric identification of organic compounds*, John Wiley & Sons, 2014.
53 C. Janiak, *J. Chem. Soc., Dalton Trans.*, 2000, 3885–3896.
54 J.-J. Wang, Z. Chang and T.-L. Hu, *Inorg. Chim. Acta*, 2012, **385**, 58–64.
55 J.-J. Wang, C.-S. Liu, T.-L. Hu, Z. Chang, C.-Y. Li, L.-F. Yan, P.-Q. Chen, X.-H. Bu, Q. Wu and L.-J. Zhao, *CrystEngComm*, 2008, **10**, 681–692.
56 S. Wang, H.-C. Su, L. Yu, X.-W. Zhao, L.-W. Qian, Q.-Y. Zhu and J. Dai, *Dalton Trans.*, 2015, **44**, 1882–1888.
57 A. J. Calahorro, E. San Sebastián, A. Salinas-Castillo, J. M. Seco, C. Mendicute-Fierro, B. Fernández and A. Rodríguez-Diéguez, *CrystEngComm*, 2015, **17**, 3659–3666.
58 J. M. Harrowfield, N. Lugan, G. H. Shahverdizadeh, A. A. Soudi and P. Thuéry, *Eur. J. Inorg. Chem.*, 2006, 389–396.
59 E. A. Mikhalyova, A. V. Yakovenko, M. Zeller, M. A. Kiskin, Y. V. Kolomzarov, I. L. Eremenko, A. W. Addison and V. V. Pavlishchuk, *Inorg. Chem.*, 2015, **54**, 3125–3133.
60 Y. Shao, G.-Z. Yin, X. Ren, X. Zhang, J. Wang, K. Guo, X. Li, C. Wesdemiotis, W.-B. Zhang and S. Yang, *RSC Adv.*, 2017, **7**, 6530–6537.
61 Y. Yan, N. N. Zhang, R. Li, J. G. Xu, J. Lu, F. K. Zheng and G. C. Guo, *Eur. J. Inorg. Chem.*, 2017, 3811–3814.
62 M. Schaer, F. Nüesch, D. Berner, W. Leo and L. Zuppiroli, *Adv. Funct. Mater.*, 2001, **11**, 116–121.
63 F. So and D. Kondakov, *Adv. Mater.*, 2010, **22**, 3762–3777.
64 M.-R. Fathollahi, F. A. Boroumand, F. Raissi and M.-J. Sharifi, *Org. Electron.*, 2012, **13**, 905–913.
65 M.-R. Fathollahi, M.-J. Sharifi, F. A. Boroumand, F. Raissi and E. Mohajerani, *J. Photonics Energy*, 2015, **5**, 057610.
66 D. D. Perrin, *Purification of laboratory chemicals*, 1980.
67 D. R. SAINT, *Bruker Analytical X-ray Systems*, Madison, Wisconsin, USA, 1997, 2006.
68 G. M. Sheldrick, *Program SADABS: Area-detector absorption correction*, University of Göttingen, Germany, 1996.
69 G. M. Sheldrick, *Acta Crystallogr., Sect. A: Found. Crystallogr.*, 2008, **64**, 112–122.
70 K. Brandenburg, *Diamond (Version 3.2), Crystal and Molecular Structure Visualization*, Crystal Impact – K. Brandenburg & H. Putz Gbr, Bonn (Germany), 2009.
71 M. Janghouri, E. Mohajerani, M. M. Amini and E. Najafi, *Appl. Phys. A*, 2014, **114**, 445–451.
72 B. Ma, B. J. Kim, L. Deng, D. A. Poulsen, M. E. Thompson and J. M. Fréchet, *Macromolecules*, 2007, **40**, 8156–8161.
73 H. Shahroosvand, L. Najafi, E. Mohajerani, A. Khabbazi and M. Nasrollahzadeh, *J. Mater. Chem. C*, 2013, **1**, 1337–1344.
74 H. Shahroosvand, L. Najafi, A. Sousaraei, E. Mohajerani and M. Janghouri, *J. Mater. Chem. C*, 2013, **1**, 6970–6980.